Bridge Maintenance, Safety, Management, Digitalization and Sustainability – Jensen, Frangopol & Schmidt (eds)

Effectiveness of geotechnical seismic isolation for post-tensioned rocking piers

A. Contento & B. Briseghella
Fuzhou University, Fuzhou, Fujian, China

A. Di Egidio & A. Aloisio
University of L'Aquila, L'Aquila, Italy

H.-H. Tsang
Swinburne University, Melbourne, Australia

P. Gardoni
University of Illinois Urbana-Champaign, Urbana, Illinois, U.S.A.

ABSTRACT: Post-tensioned (PT) rocking piers have received considerable attention as an advantageous solution for seismic resilient structures. Their self-centering capacity, the advantages related to the column-uplifting mechanisms, and the possibility of being combined with energy dissipation devices largely contributed to this increasing attention. Simultaneously, Geotechnical Seismic Isolation (GSI) has emerged as a technique to reduce the seismic vulnerability of structures. The GSI a technique is based on design of a suitable interface between the foundation of the structure and the surrounding terrain. Such an interface can work as seismic isolation and energy dissipation mechanism. This research investigates the use of GSI for PT rocking piers equipped with external energy dissipation devices. The main focus of the investigation is the comparative assessment of the effectiveness of external dissipators and GSI to ascertain if the two protection mechanisms can synergize and collaboratively enhance the safety of the structure. The investigation employs numerical simulations through the direct integration of the equation of motion of the studied system. The outcomes of the parametric analysis are presented in gain maps that illustrate the effectiveness of the coupling within a designated parameter plane. Preliminary results show that GSI could be effective in combination with external dampers in reducing the seismic effects on rocking piers.

1 INTRODUCTION

Historically, self-centering structures have been widely used as seismic-resistant structures for their limited residual displacements. Additionally, starting from the last decades of the previous century, particular attention has been paid to rocking structural systems, and a significant number of researchers tried to make full use of their gravity-recentering ability for the design of seismic-resistant structures. The category of rocking structural systems comprises a variety of structures, the most common being rocking podiums, rocking frames and walls, and rocking piers. The inherent self-centering and energy dissipation abilities of rocking structural systems can be enhanced with the addition of supplementary devices aimed at reducing the displacement seismic demand of such structures and, consequently, mitigate their possible damage.

In the case of rocking piers, which are the focus of the present study, the seismic response is usually improved with three main protection strategies: *i*) base isolation (Rele et al., 2021), *ii*) use of internal post-tensioned (PT) tendons (Liu et al., 2018), *iii*) use of connection elements with dissipative behaviour at the rocking interface or external dissipative devices (EDDs) (Li et al., 2021, Sarti et al., 2016). Such a classification is proposed solely for the sake of clarity

DOI: 10.1201/9781003483755-478

since, in most cases, multiple strategies are applied at the same time in order to obtain dissipative controlled rocking. Both Zhong & Christopoulos (2022) and Piras et al. (2022) provide extensive literature reviews on rocking piers. The first one contains a comprehensive overview of self-centering rocking structures and focuses more on experimental works, whereas the second focuses on rocking bridge substructure systems and reviews other dissipation solutions proposed in the literature.

Relatively recently, Geotechnical Seismic Isolation (GSI) has emerged as a technique to reduce the seismic vulnerability of structures (Tsang 2008). Differently from the protection strategies presented above, GSI does not directly modify the characteristics of the structure to be protected but works on the interface between the foundation of the structure and the surrounding terrain. Thus, the main protection mechanism is based on the modification of the soil-structure interaction. Engineered soils, geosynthetics (geogrids, geotextiles), and granular materials like sand and gravel are commonly used in GSI systems. Their properties are tailored to achieve the desired isolation effect. GSI systems mostly involve three main protection mechanisms for the main structure. The first uses the modified foundation soil to alter the system's dynamic response by shifting its fundamental frequency (Aloisio et al. 2022, Tsang 2023). This mechanism is usually realized either through a layer of low-modulus material or through a sliding interface and its conceptual base is the same as the traditional base isolation mechanism. The second protection mechanism uses the dissipative properties of the engineered soil to reduce or filter the energy directed to the structure (Hazarika et al. 2023). The third mechanism relies on deliberate sliding control between the structural foundation and the encompassing geomaterials (Banović et al. 2022).

This paper proposes an initial investigation into the possible improvement in the seismic behaviour of rocking piers due to the application of EDDs and GSI. In particular, the focus is on the evaluation of the relative effectiveness of the two protection strategies. The authors aim to ascertain if the effectiveness of GSI is comparable to that of EDDs and if the two protection strategies can synergize and lead to a significant improvement in the seismic dynamics of rocking piers when used simultaneously. The model of a pier with a single unbound post-tensioned tendon located in the center of its cross-section and equipped with two viscous EEDs and GSI is used for the investigation. The GSI is modeled as in Tsang (2023) where the foundation is connected to the ground with both translational and rotational springs and dashpots. The models for the cases where EDDs or GSI are not considered are obtained from this reference model removing the unneeded terms in the equations of motion. The equations of motion of the reference structure (i.e. the pier with both EDD and GSI) are derived through a Lagrangian approach. The impact conditions needed to complete the mathematical model follow from the assumption of the conservation of the angular and linear momenta. The investigation employs numerical simulations through the direct integration of the equation of motion of the studied system. The outcomes of the parametric analysis are presented in maps that illustrate the maximum rotation of the pier with respect to the critical rotation that would lead to the pier overturning. Preliminary results show that GSI could be effective in combination with external dampers in reducing the seismic effects on rocking piers.

2 ROCKING PIER MODEL AND GSI MODELS

The pier investigated in this paper is modeled as a rigid block linked to a rigid oscillating base and to an additional mass at its top. The oscillating base represents the pier's foundation, and the connection is established through two viscous dampers. The additional mass schematizes the substructure above the pier, encompassing the deck and any other supplementary mass. Such a mass is assumed to remain horizontal during the motion.

In the case of GSI, the setup originally suggested by Tsang (2008) is adopted. As shown in Figure 1a, in this configuration, the base of the pier is embedded in a layer of low-modulus material, providing simultaneous support and confinement to the rigid base. These two elements are assumed to move cohesively in response to external excitation. Conversely, when GSI is not considered, the low-modulus material layer is replaced with a layer of natural soil (NS). The effect of

the layer of low-modulus material is modeled through two couples of springs and dashpots (Figure 1b) that act on the translation and rotation of the foundation of the pier, respectively.

Concerning the pier, the geometric configuration of the rigid block is that of a symmetric parallelepiped with a base of $2b_p$, a height of $2h_p$, and a unitary depth of $d_p = 1$, orthogonal to the representation of Figure 1b. The position of the center of mass of the pier m_p, denoted as G_p (Figure 1b and d), aligns with the geometric center of the parallelepiped, assuming uniform material composition with mass density ρ.

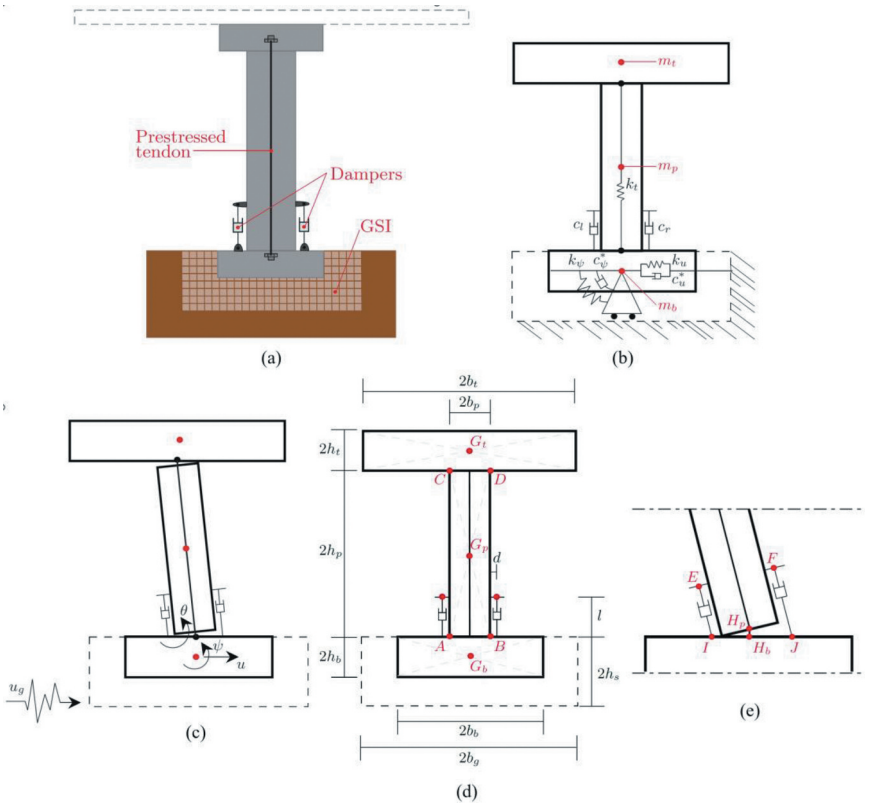

Figure 1. Schematic representation of the studied system (a); positions of the centers of masses; springs and dashpots used in the model (b); positive directions of the Lagrangian parameters (c); notable points used to describe the behavior of the pier (d) and (e).

In the proposed model, it is assumed that both free flight and sliding are prevented. Given this assumption, three distinct phases of motion can occur: rest, full contact, and rocking. The rest phase is the simplest, where neither the pier nor the oscillating base undergoes relative displacements with the soil. In the full contact phase, the oscillating base moves with respect to the ground, but there is no rocking of the pier. Finally, in the rocking phase, both base oscillation and rocking occur simultaneously. The equations of motions of the rocking phase can be written considering three Lagrangian parameters: the rocking angle $\theta = \theta(t)$, the rotation of the oscillating base $\psi = \psi(t)$, and its translational displacement $u = u(t)$. Figure 1c shows the positive directions of these Lagrangian parameters. The equations of motions of the other phases can be derived from the equations of motions of the rocking phase by removing unnecessary terms and equations.

2.1 *Equations of motion*

This section presents the derivation of the equations of motion for the complete rocking in the case of rocking occurring around point A (i.e. the bottom left vertex of the rigid body); those for rocking occurring around point B can be derived with the same approach and are not

presented for the sake of brevity. The equations of motion of the rocking pier are obtained by the well-known Lagrange's equation

$$\frac{d}{dt}\left(\frac{\partial L(t)}{\partial \dot{q}_l(t)}\right) - \frac{\partial L(t)}{\partial q_i(t)} = Q_i(t), \tag{1}$$

where the Lagrangian $L(t) = T(t)$-$V(t)$ is the difference between kinetic energy $T(t)$ and potential energy $V(t)$, $q_i(t)$ is one of the three Lagrangian parameters, and $Q_i(t)$ is the non-potential forces corresponding to $q_i(t)$. The kinetic energy $T(t)$ can be derived as

$$\begin{aligned} T(t) = \tfrac{1}{2}\big[&\big(J_b + J_p + J_t\big)\big(\dot{\boldsymbol{\Psi}}(t)\cdot\dot{\boldsymbol{\Psi}}(t)\big) + J_p\big(\dot{\boldsymbol{\theta}}(t)\cdot\dot{\boldsymbol{\theta}}(t)\big) + \\ &m_b(\dot{\mathbf{x}}_{G_b}(t)\cdot\dot{\mathbf{x}}_{G_b}(t)) + m_p\big(\dot{\mathbf{x}}_{G_p}(t)\cdot\dot{\mathbf{x}}_{G_p}(t)\big) + m_t(\dot{\mathbf{x}}_{G_t}(t)\cdot\dot{\mathbf{x}}_{G_t}(t))\big]. \end{aligned} \tag{2}$$

In Equation 2, J_b, J_p, and J_t are the polar inertia of the oscillating base, column, and top mass with respect to their centers of mass. The rotation vectors $\boldsymbol{\psi}(t)$ and $\boldsymbol{\theta}(t)$ are defined as $\boldsymbol{\psi}(t) = \{0,\ 0,\ \psi(t)\}^{\mathrm{T}}$ and $\boldsymbol{\theta}(t) = \{0,\ 0,\ \theta(\mathrm{i})\}^{\mathrm{T}}$, respectively. Vectors $\mathbf{x}_{Gb}(t)$, $\mathbf{x}_{Gp}(t)$, and $\mathbf{x}_{Gt}(t)$ define the positions of the respective centers of mass referred to an inertial reference system with an origin that is initially coincident with the left base vertex of the rigid block, i.e. point A in Figure 1b. They are functions of the Lagrangian parameters ($u(t)$, $\psi(t)$, and $\theta(t)$) and of the external ground excitation $x_g(t)$.

The potential energy $V(t)$ reads:

$$\begin{aligned} V(t) = &\big[m_p\big(\mathbf{x}_{G_p}(t) - \mathbf{x}_{G_p}(0)\big) + m_t(\mathbf{x}_{G_t}(t) - \mathbf{x}_{G_t}(0))\big]\cdot g + \frac{1}{2}[k_u(\boldsymbol{u}(t)\cdot\boldsymbol{u}(t)) + \\ &k_\psi(\boldsymbol{\psi}(t)\cdot\boldsymbol{\psi}(t)) + 2\big\|\mathbf{x}_{H_p}(t) - \mathbf{x}_{H_b}(t)\big\|\cdot\big(2k_t\big\|\mathbf{x}_{H_p}(t) - \mathbf{x}_{H_b}(t)\big\| + \sigma_0\big)\big]\ , \end{aligned} \tag{3}$$

with $g = \{0,\ g,\ 0\}^{\mathrm{T}}$ and $u(t) = \{u(t),\ 0,\ 0\}^{\mathrm{T}}$, where g is the gravity acceleration. In the equation, k_u and k_ψ are the translational and rotational stiffness coefficients of the GSI, whereas k_t is the axial stiffness of the unbound tendon. Vectors $\mathbf{x}_{Hp}(t)$ and $\mathbf{x}_{Hb}(t)$ provide the positions of the middle point of the base of the rigid block (i.e. point H_p in Figure 1c) and the position of the corresponding point on the oscillating base H_b. Consequently, the norm $\big\|\ \mathbf{x}_{Hp}(t) - \mathbf{x}_{Hb}(t)\big\|$ corresponds to half of the elongation of the unbound tendon due to rocking. Lastly, σ_0 is the prestress in the unbound tendon.

Since all non-conservative forces are dissipative forces, it is possible to write the non-potential forces $Q_i(t)$ in terms of a dissipative function $R(t)$ as $Q_i(t) = -\partial R(t)/\partial \dot{q}_i\,(t)$. Such dissipative function accounts for the viscous damping due to the GSI and external dampers and is written as

$$\begin{aligned} R(t) = &\frac{1}{2}\big[c_\psi(\dot{\boldsymbol{\psi}}(t)\cdot\dot{\boldsymbol{\psi}}(t)) + c_u(\dot{\mathbf{u}}(t)\cdot\dot{\mathbf{u}}(t)) + c_l\frac{d}{dt}(\|\mathbf{x}_{\mathrm{E}}(t) - \mathbf{x}_I(t)\| - \\ &\Big\|\mathbf{x}_E(\mathbf{0}) - \mathbf{x}_I(\mathbf{0})\|\Big)^2 + C_r\frac{d}{dt}\Big(\Big\|\mathbf{x}_F(\mathbf{t}) - \mathbf{x}_J(\mathbf{t})\| - \Big\|\mathbf{x}_F(\mathbf{0}) - \mathbf{x}_J(\mathbf{0})\|\Big)^{\mathbf{2}}, \end{aligned} \tag{4}$$

where c_u and c_ψ are the dissipative coefficients of the GSI model, whereas c_l and c_r are the dissipative coefficients of the left and right external viscous dampers, respectively. In Equation 4, the terms multiplied by c_l and c_r represent the time derivative of the elongation of the two dampers.

To complete the mechanical model, uplift and impact conditions are also derived. The uplift occurrence is verified by comparing the total translational acceleration acting on the column during integration in the full-contact phase (i.e. the total acceleration on the column computed from the full-contact equations) with the total acceleration acting on the column in the case of incipient uplift (i.e. the total acceleration computed from the rocking equations, where θ and it two first time derivative are neglected). The impact conditions, which provide the values of the Lagrangian parameters after an impact are derived by imposing the conservation of *i*) the angular momentum around the rocking vertex of the column, *ii*) the angular momentum around the center of rotation of the base of the pier, and *iii*) the conservation of

the horizontal momentum. Solving the three conservation equations, it is possible to find the post-impact values $u(t_i^+)$, $\theta(t_i^+)$, and $\psi(t_i^+)$ as functions of the post-impact quantities $u(t_i^-)$, $\theta(t_i^-)$, and $\psi(2t_i^-)$.

2.2 *Geotechnical seismic isolation model*

The model presented by Tsang & Pitilakis (2019) is used to model the basic configuration of the GSI system first proposed by Tsang (2008). Such a configuration assumes that the foundation of the pier is completely embedded in a layer of low-modulus material. The GSI layer has the shape of a rectangular prism of dimensions $2b_{\mathrm{GSI}}\times 2h_{\mathrm{GSI}}\times 2d_{\mathrm{GSI}}$, where $2d_{\mathrm{GSI}}$ is the dimension orthogonal to the schematic cross-section shown in Figure 1d. This paper assumes that the material used for the GSI is a rubber–soil mixture (RSM), which is usually widely proposed in the literature because of its compatibility with the natural environment and the availability of materials. The characteristics of such material (i.e. small-strain shear modulus $G_{max,\mathrm{GSI}}$, density ρ_{GSI}, and Poisson's ratio ν_{GSI}, as well as the characteristics of the natural soil that it replaces (i.e $G_{max,\mathrm{NS}}$, ρ_{NS}, and ν_{NS}) are also taken from Tsang & Pitilakis (2019).

The mechanical behaviour of the GSI is modeled by two sets of springs and dashpots. The first one, with stiffness and damping coefficients denoted as k_u and c_u, acts on the translation degree of freedom u. Similarly, the second one, which has coefficients denoted as k_ψ and c_ψ, works on the rotation ψ and its first derivative with respect to time. All of the four coefficients are functions of the geometric and mechanic characteristics of the GSI system (i.e., b_g, h_g, d_g, $G_{max,\mathrm{GSI}}$, ρ_{GSI}, and ν_{GSI}). Following Tsang (2023), k_u is modeled as:

$$k_u = k_b f_t f_w f_{lx} f_{lex}. \tag{5}$$

The stiffness coefficient k_b originates from the shearing interaction between the foundation base and the underlying soil. The effect of the embedment depth D is accounted for by f_t, whereas f_w, instead, accounts for the lateral interaction between embedded foundation walls and surrounding material. The last two, f_{lx} and f_{lex}, are additional stiffening factors, that account for the underlying stiffer layer of the NS and an additional embedment effect.

The damping coefficient c_u is modeled as:

$$c_u = k_u \frac{\xi_{eq} T_{SSFS}}{\pi} + c_b + c_s + c_p \tag{6}$$

The first term is the coefficient of the equivalent linear viscous damping due to the material internal damping that accounts for the hysteretic behaviour of the material. In Equation 6, ξ_{eq} is the equivalent viscous damping coefficient and T_{SSFS} is the fundamental natural period of the structure. It should be noted that the value of T_{SSFS} for a rocking structure is purely conventional since the column is modeled as a rigid body and not as a flexible structure The other three terms model the radiation damping which accounts for the energy loss as elastic waves propagate away from the foundation into an open half-space. Specifically, c_b refers to the shear generated between the base of the foundation and the soil, c_s to the shear between the lateral surfaces of the foundation in the direction of the motion and the soil, and c_p to the pounding due to the two lateral surfaces of the foundation in the direction orthogonal to the motion.

The rotation stiffness coefficient k_ψ is also expressed as the product of multiple factors as:

$$k_\psi = k_r \alpha_\psi f_{emb} f_{l\psi} f_{le\psi}. \tag{7}$$

In Equation 7, the rotational stiffness of the surface foundation k_r is conceptually analogous to k_b Such a rotational stiffness is multiplied by dynamic stiffness modifier α_0 which is dependent on T_{SSFS}. Both f_{emb} and $f_{le\psi}$ are stiffening factors that are functions only of the geometry of the GSI system and in particular of D. Lastly, $f_{le\psi}$ accounts for a further stiffening effect due to the stiffer original NS that underlies the low-modulus GSI layer.

Lastly, the damping coefficient c_ψ is modeled as:

$$c_\psi = k_\psi \frac{\xi_{eq} T_{SSFS}}{\pi} + c_r + c_{emb}. \tag{8}$$

As in Equation 6, the first term of Equation 8 corresponds to the equivalent linear viscous damping due to the material internal damping. The damping coefficient c_r, instead, refers to the rocking of the surface foundation. The last term,c_{emb}, accounts for the interaction of the lateral walls of the foundation with the surrounding material that generates compression-extension waves, shear weaves, and torsional weaves. The explicit definition of the four coefficients, as well as the exact definition of each of their factors/terms, can be found in Tsang & Pitilakis (2019).

3 PRELIMINARY ANALYSES

This paper presents the initial result of a larger campaign of parametric analyses performed to understand the influence of the geometric and mechanic characteristics of PT tendon, EDDs, and GSI on the seismic behaviour of the rocking pier. For this purpose, the ground motion record of the 1994 Northridge earthquake used in Tsang & Pitilakis (2019) is considered as seismic input. The seismic record is scaled to have a PGA = 1g. The dimensions of the column used in the following analyses are $2b_p$ = 0.5m and $2h_p$ = 4m; whereas the dimensions of the pier's foundations are $2b_b$ = 1.5m, $2h_b$ = 0.8m, and d_b = 2m. The mass of the superstructure is set to m_t = 10,400kg and the damping coefficient of the EDDs to $c_r = c_l$ = 225kNs/m. The mechanical characteristics of the RSM layer are $G_{max,GSI}$ = 5.88MPa, ρ_{GSI} = 1200kg/m^3, and ν_{GSI} = 0.4, while those of the NS are $G_{max,NS}$ = 120.3 MPa, ρ_{NS} = 1600kg/m^3, and ν_{NS} = 0.4. The reference values for the diameter and prestress of the PT tendons are d_{ten} = 10.0mm and respectively. The reference dimensions of the RSM layer are $2b_{GSI}$ = 1.7m, $2h_{GSI}$ = 2m, and $2d_{GSI}$ = 2.2m.

The first analysis, whose results are shown in Figure 2, is used to evaluate the sensitivity of the compared mechanical systems to the characteristics of the PT tendon. In particular, three different mechanical systems are compared: the rocking pier without EDDs and GSI (Figure 2a), the rocking pier equipped with EDDs (Figure 2b), and the rocking pier equipped with both EDDs and GSI (Figure 2c). For all the three systems the diameter of the PT tendon d_{ten} is varied between 5mm and 25mm while the prestress covers the range $\sigma_0 = 5{\cdot}10^6$ -$50{\cdot}10^6$N. For each combination of values, the equations of motion are integrated and the maximum total rotation of the pier $\zeta = \max(\psi + \theta)$ is collected. The metric used to represent the results is the ratio between this value and the critical angle of the column $\alpha_{crit} = \text{arctg}(b_b/h_b)$, i.e. $\Delta\zeta = \zeta/\alpha_{crit}$. Such a ratio corresponds to the percentage of the capacity of the column assuming the overturning as the limit state. This choice is made to provide a reference for the comparison; in an actual structure, the maximum rotation would be constrained by other factors such as the maximum elongation of the EDDs as well as the maximum lateral displacement allowable for the superstructure.

Figure 2a shows that when DDEs and GSI are not considered the seismic behaviour of the pier in terms of maximum rotation is negligibly affected by the value of the prestress in the tendon, especially for higher values of the stiffness of the tendon that is proportional to d_{ten}. That can be understood by noticing that the contour plots are almost vertical; for a given value of d_{ten} the difference in $\Delta\zeta$ can be attributed to the nonlinearity of the problem. Differently, the values of $\Delta\zeta$ strongly decrease as d_{ten} increases up to a value of approximately 12mm; after such a value the dependence of $\Delta\zeta$ on d_{ten} is largely reduced and the maximum angle reached during the motion is approximately 35% of the critical angle. When the EDDs are introduced into the system (Figure 2b), the maximum rotation reached by the pier during the motion reduces. Such a reduction is larger for smaller values of d_{ten} for which an approximate 10% reduction in $\Delta\zeta$ occurs. The reduction decreases after the threshold value of d_{ten} = 12mm to about 5% of the value reached without EDDs. The results still appear not to be significantly affected by σ_0, and this tendency is confirmed even when the GSI is considered (Figure 2c). Figure 2c shows that the combined effect of DDEs and GSI largely reduces the values of $\Delta\zeta$, especially for low values d_{ten} with the maximum value of $\Delta\zeta$ that drops from 0.685 in Figure 2a to 0.375 in Figure 2c. The introduction of the GSI further reduces the dependence of $\Delta\zeta$ on d_{ten}. However, smaller values of can be observed for smaller d_{ten} and a relative minimum can be roughly observed for 22mm < d_{ten} < 23mm.

The second analysis, presented in Figure 3, compares the seismic behaviour of the systems equipped with GSI for different base dimensions of the RSM layer. Figure 3a refers to the system with GSI and without EDDs, while Figure 3b refers to the system with both GSI and EDDs. Both the longitudinal and the orthogonal base dimensions of the RSM layer start from values that correspond to those of the pier's foundation plus 10cm for each side and are increased up to exceed the dimensions of the pier's foundation of 1m (i.e. 50cm for each side).

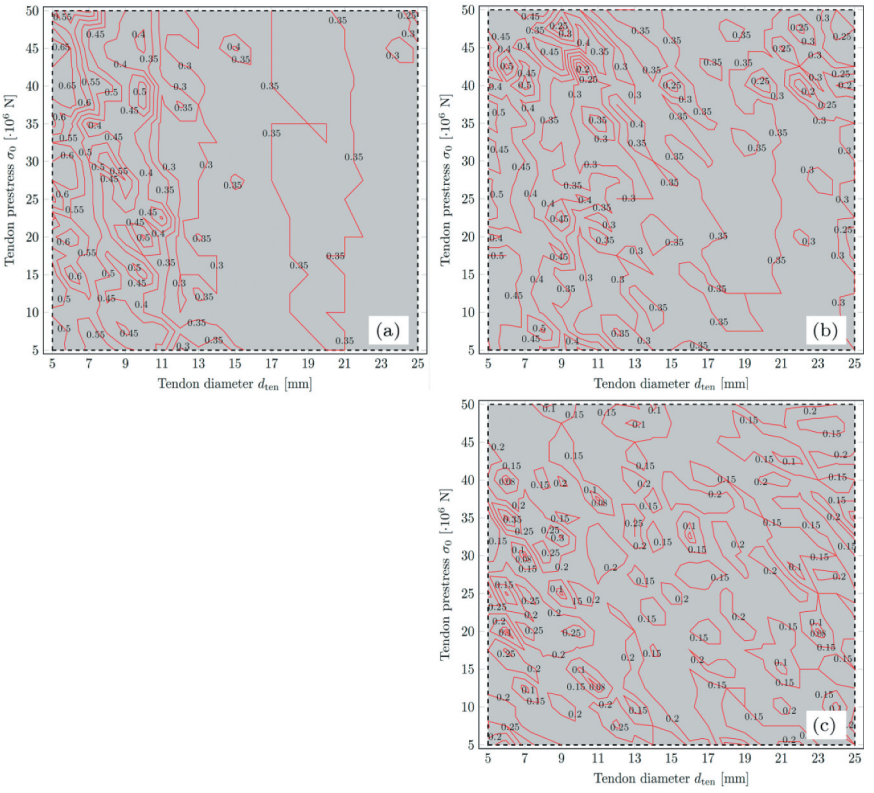

Figure 2. Contour plots of $\Delta\zeta$ as a function of the diameter and prestress of the PT tendon: (a) rocking pier; (b) system with EDDs; (c) system with GSI and EDDs.

Figures 3a and 3b show that although the dimensions of the RSM layer affect the values of the four parameters that characterize the GSI, there are only minor changes in the maximum rotation of the pier compared to the results of Figure 2c. Additionally, the comparison of the two graphs in Figure 3 clarifies that the effect of the EDDs is limited and almost negligible. However, the introduction of the EDDs changes the values for which the minimum values of $\Delta\zeta$ are obtained. There are concurrent reasons that justify this evidence. The first one is that the reduction due to the GSI for this seismic input is so high that there is no room to evaluate the effectiveness of the EDDs; this is shown by the small values assumed by $\Delta\zeta$ in all the parameters' plane. The second reason is that the GSI reduces the time spent in the rocking phase and, since for the chosen seismic inputs the maximum rotation occurs soon after the uplift, there is not enough time to benefit from the effects of the EDDs that are more evident later in the motion. However, this finding should be confirmed by assuming in the analyses different values of the EDDs' damping coefficients. Although limited, the initial analyses presented in this paper justify the necessity to further investigate the possibility of adopting the GSI as a protection mechanism for rocking piers with and without the addition of EDDs.

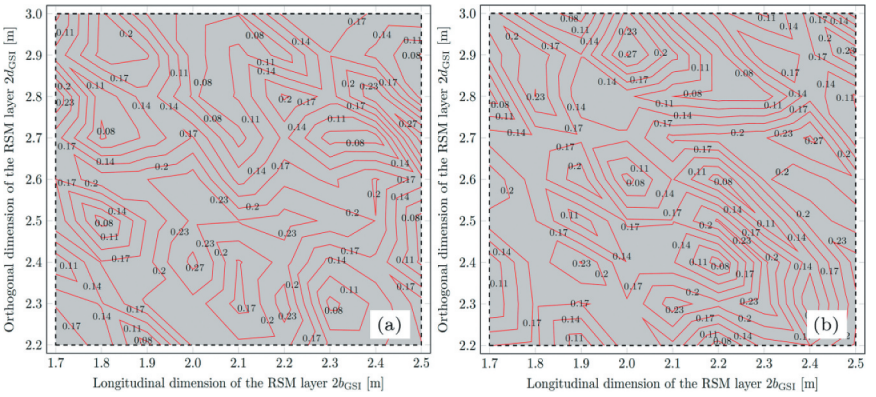

Figure 3. Contour plots of $\Delta\zeta$ as a function of the geometric characteristics of the RSM layer: (a) system with GSI; (b) system with GSI and EDDs.

4 CONCLUSIONS

The present study focuses on the seismic protection of PT rocking piers through GSI. In particular, through detailed models and computer simulations, the study scrutinizes the collaborative potential of GSI and EDDs in improving the resilience of rocking piers. Preliminary findings obtained through parametric analyses suggest a positive impact when GSI and EDDs collaborate. This discovery hints at a potential way to enhance the safety of bridges during earthquakes and contributes to ongoing discussions about earthquake-resistant design, paving the way for further exploration and testing in real-world scenarios.

REFERENCES

Aloisio, A., Contento, A., Xue, J., Fu, R., Fragiacomo, M. & Briseghella, B. 2022. Probabilistic formulation for the q-factor of piles with damping pre-hole. *Bulletin of Earthquake Engineering* 21(8): 3749–3775.

Banović, I., Radnić, J., Grgić, N. & Semren, K. 2023. Effectiveness of several low-cost geotechnical seismic isolation methods: a shake-table study. *Bulletin of Earthquake Engineering* 21(8): 3923–3947.

Hazarika, H., Kuribayashi, K., Kuroda, S. & Hu, Y. 2023. Performance evaluation of waste tires in protecting embankment against earthquake loading. *Bulletin of Earthquake Engineering* 21(8): 4019–4035.

Li, Y., Li, J., & Shen, Y. 2021. Quasi-static and nonlinear time-history analyses of post-tensioned bridge rocking piers with internal ED bars. *Structures* 32: 1455–1468.

Liu, X., Li, J., Tsang, H.H., & Wilson, J. 2018. Enhancing seismic performance of unbonded prestressed concrete bridge column using superelastic shape memory alloy. *Journal of Intelligent Material Systems and Structures* 29: 3082–3096.

Piras, S., Palermo, A., & Saiidi, M.S. 2022. State-of-the-art of posttensioned rocking bridge substructure systems. *Journal of Bridge Engineering* 27: 03122001.

Rele, R., Balmukund, R., Bhattacharya, S., Cui, L., & Mitoulis, S.A. 2021. Application of controlled-rocking isolation with shape memory alloys for an overpass bridge. *Soil Dynamics and Earthquake Engineering* 149: 106827.

Sarti, F., Palermo, A., & Pampanin, S. 2016. Fuse-type external replaceable dissipaters: Experimental program and numerical modeling. *Journal of Structural Engineering* 142: 04016134.

Tsang, H.H. 2008. Seismic isolation by rubber–soil mixtures for developing countries. *Earthquake Engineering & Structural Dynamics* 37(2):283–303.

Tsang, H.H. 2023. Analytical design models for geotechnical seismic isolation systems. *Bulletin of Earthquake Engineering* 21(8): 3881–3904.

Tsang, H.H. & Pitilakis, K. 2019. Mechanism of geotechnical seismic isolation system: Analytical modeling. *Soil Dynamics and Earthquake Engineering* 122: 171–184.

Zhong, C. & Christopoulos, C. 2022. Self-centering seismic-resistant structures: Historical overview and state-of-the-art. *Earthquake Spectra* 38: 1321–1356.